ELSEVIER

Thermochimica Acta 264 (1995) 219–230

thermochimica acta

Thermal decomposition of zinc–iron citrate precursor

N.S. Gajbhiye [a,1], U. Bhattacharya [b], V.S. Darshane [b,*]

[a] *Department of Chemistry, University of Bombay, Vidyanagari, Bombay-400 098, India*
[b] *Department of Chemistry, The Institute of Science, Bombay-400 032, India*

Received 6 July 1994; accepted 25 February 1995

Abstract

A citrate precursor technique has been used to synthesize ultrafine particles of zinc ferrite ($ZnFe_2O_4$). The precursor, $Zn_3Fe_6(C_6H_5O_7)_8 \cdot (12 + n)H_2O$, was studied using thermoanalytical techniques. It was found that decomposition in air was suitable for obtaining $ZnFe_2O_4$. The thermal decomposition involved seven steps, with the citrate precursor first losing the adsorbed and coordinated water molecules. In subsequent steps, the citrate groups lost water molecules to form metal aconitates, which further decomposed in the temperature range 260–320°C to give hydrozincite and FeO·OH. These intermediates decomposed further with the formation of ZnO and Fe_2O_3, along with the evolution of CO_2 and H_2O. A further step involved the formation of $ZnFe_2O_4$ in the temperature range 460–560°C at the expense of the ZnO and Fe_2O_3 phases. The citrate precursor and decomposed products were analysed by IR and X-ray diffraction techniques.

Keywords: Ferrite; IR; Particle size; Precursor; TA

1. Introduction

Fine-grained spinel ferrite materials are of vital technological interest due to their applications in the preparation of high-density ferrites at low temperatures, suspension materials in ferromagnetic liquids [1] and catalysts [2, 3–4]. To produce ultrafine particles of ferrites artificially, one may utilize various techniques, such as co-precipitation, freeze drying, spray drying, or the sol-gel process, including some recent innovations [5–9]. The conventional ceramic method for the preparation of ferrites requires high sintering temperatures and results in the loss of the

[1] On leave from the Department of Chemistry, I.I.T., Kanpur-208 016, India.
* Corresponding author.

SSDI 0040-6031(95)02331-3

fine-particle nature. Thermal decomposition of oxalate solid-solution precursors [10] and combustion/decomposition of the solid solution precursors of metals, like the hydrazinium metal hydrazine carboxylate hydrates, are reported to yield fine-particle ferrites [11]. Very recently, modifications of the sol-gel process have been used to produce submicrometre-sized $NiFe_2O_4$ particles, which were of uniform size and shape, by hydrolysis of an alkoxide aerosol [7, 8]. The decomposition of dysprosium ferric citrate precursor leads to the formation of ultrafine $Dy_3Fe_5O_{12}$, and other rare earth iron garnet materials have been formed from their citrate precursors [12, 13].

A literature survey showed that no systematic efforts have been made to investigate the thermal decomposition of citrate precursors as a means of preparation of ultrafine zinc ferrite spinels. Therefore, the present investigation was undertaken to prepare ultrafine $ZnFe_2O_4$ and to study the mode of thermal decomposition of the citrate precursor.

2. Materials and methods

2.1. Preparation of the zinc–iron(III) citrate precursor

Zinc oxide (1.6878 g) from Aldrich (99.99%) was dissolved in 50 ml of 6 N nitric acid (Glaxo, AnalaR). After the formation of a clear solution of zinc nitrate, the solution was evaporated to dryness and dissolved in 50 ml of distilled water. This solution was evaporated to remove excess nitric acid. The calculated amount of iron(III) citrate (12.2304 g; Emerck, AnalaR) was dissolved in a minimum amount of warm distilled water with constant stirring and then added to the zinc nitrate solution to maintain Zn and Fe in the molar ratio 1:2. Then 2.6545 g of anhydrous citric acid (BDH, AnalaR) was dissolved in 100 ml of water in a separate beaker and later added to the above solution. This mixture containing Zn, Fe and citric acid in the molar ratio 1:2:2.33 was further refluxed for 5 h at 100°C. Finally, the refluxed solution was slowly evaporated and then transferred to a petri-dish to form a gel. This gel was dehydrated in an oven at 110°C to obain the zinc–iron citrate precursor. During the dehydration process, the gel turned into a fluffy mass, which then crumbled to a powder.

2.2. Analysis of the citrate precursor

The iron content of the precursor was estimated gravimetrically. A solution of the precursor was made highly acidic (pH 3) by addition of concentrated HCl, and cooled to 10°C. Aqueous 5% cupferron solution was added until the formation of the brown precipitate was complete. This precipitate was filtered and later incinerated to obtain Fe_2O_3. Zinc was estimated by titrating the solution (maintained at pH 10) against EDTA using Solochrome Black as indicator [14]. The citrate content was estimated by titrating with 1 N NaOH, using thymol blue as an indicator [15]. The stoichiometric formula of the precursor was estimated to be $Zn_3Fe_6(Cit)_8 \cdot (12 + n)H_2O$ (where n is the number of adsorbed water molecules).

2.3. Experimental techniques

Thermal analysis of the citrate precursor was carried out at $10\,K\,min^{-1}$ in an air atmosphere up to 1000°C on a MOM derivatograph (Hungary) which recorded TG/DTG/DTA simultaneously.

A Perkin-Elmer 240 C elemental analyser was used to analyse the evolved gases.

FTIR spectra were recorded in the range $4000–400\,cm^{-1}$ using KBr as a standard.

X-ray diffractograms were recorded with Cu Kα radiation using an Ni filter. The lattice parameters and crystallite sizes were calculated from the XRD patterns [16].

A particle-size analyser (Horiba LA-500), based on Fraunhofer diffraction and Mie scattering theories, was used to determine the size of the particles.

3. Results

3.1. Effect of atmosphere on thermal decomposition

The decomposition of the citrate precursor was carried out in different atmospheres of N_2 and O_2 with compositions in the ratio (a) 0.0:100 (dry oxygen), (b) 50:50, (c) 80:20 (air) and (d) 100:0.0 (dry nitrogen). The citrate precursors were decomposed at 620°C for 8 h in these four different atmospheres. All the resultant samples showed XRD patterns for zinc ferrite ($ZnFe_2O_4$), without the presence of any extra diffraction lines that can be attributed to individual oxides. The lattice parameters calculated for samples (a)–(d) were respectively 0.8448, 0.8444, 0.8431 and 0.8438 (± 0.002) nm. It may be noted that the samples decomposed in air and dry nitrogen have lattice parameters that are very close to the reported value of 0.84265 nm [17]. This leads to the conclusion that pure $ZnFe_2O_4$ phase can be obtained by heating the precursor either in air or pure nitrogen.

3.2. Thermal decomposition of the citrate precursor

Fig. 1 shows TG, DTG and DTA curves of the citrate precursor heated in air. There are four main steps in the reaction: (i) dehydration, (ii) decomposition of citrate, (iii) decomposition of carbonate, and (iv) formation of $ZnFe_2O_4$.

Fig. 1 shows two endothermic peaks corresponding to dehydration of the citrate precursor. After dehydration, there are two endothermic and one exothermic peaks, corresponding to decomposition of citrate to carbonate. Following these peaks are an endotherm and an exotherm corresponding to the formation of $ZnFe_2O_4$ through the solid-state diffusion process ($ZnO + Fe_2O_3 \rightarrow ZnFe_2O_4$) accompanied by rearrangement in the $ZnFe_2O_4$ lattice. The observed mass losses and the corresponding temperature ranges are given in Table 1.

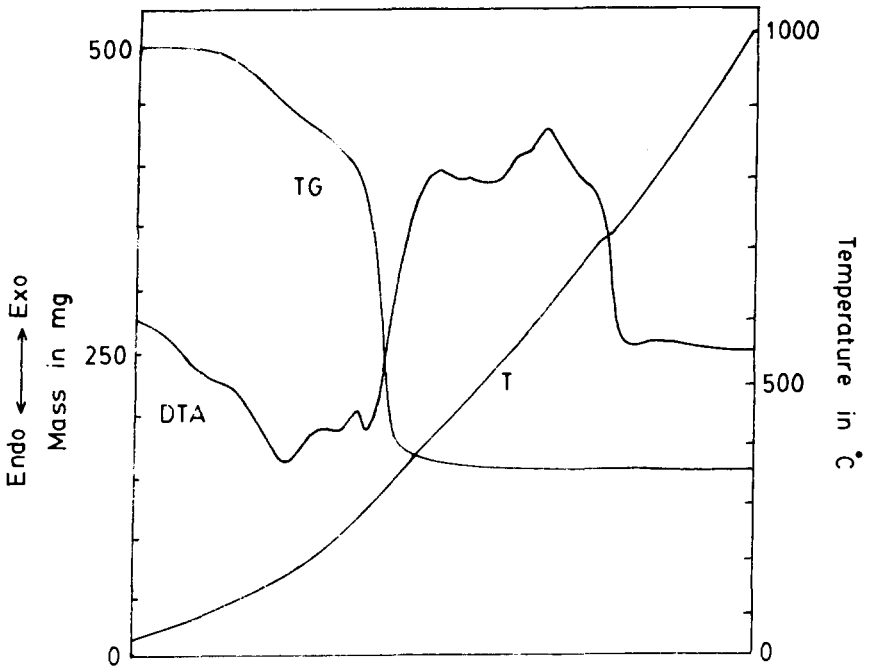

Fig. 1. TG and DTA curves of zinc–iron citrate precursor (in air).

Table 1
Mass losses in the decomposition steps of $Zn_3Fe_6(C_6H_5O_7)_8 \cdot (12+n)H_2O$

Peak temp./°C	Temperature range/°C	Loss of mass/%	Molecular formula
110	25–120	–	$Zn_3Fe_6(C_6H_5O_7)_8 \cdot 12(H_2O)$
180	120–220	9.56	$Zn_3Fe_6(C_6H_5O_7)_8$
240	220–260	6.45	$Zn_3Fe_6(C_6H_3O_6)_8$
285	260–320	45.47	$Zn_5(CO_3)_2 \cdot 6(OH) + ZnCO_3 + 12(FeO \cdot OH)$
420	320–460	4.55	$(ZnO)_6 \cdot CO_2 + (Fe_2O_3)_6 \cdot CO_2$
520	460–560	0.97	$(ZnFe_2O_4)_6 \cdot CO_2$
620	560–680	0.90	$ZnFe_2O_4$

3.3. Dehydration of the citrate precursor (85–220°C)

The number of water molecules adsorbed on the citrate precursor molecule varies depending upon the atmospheric humidity. The extra water can be removed by heating the citrate precursor at 110°C, which is shown by the endotherm between 85 and 120°C (Fig. 1). Removal of the coordinated water molecules of the citrate precursor takes

place between 120 and 220°C as shown by the second endotherm. The TG curve shows a mass loss of 9.56% which corresponds exclusively to loss of water. On the basis of the molar mass, 2043.24 g mol^{-1}, assigned to the precursor, the evolution of water corresponds to about 12 coordinated water molecules per formula unit.

3.4. Decomposition of the citrate precursor (220–460°C)

The thermal decomposition of the citrate precursor is a multistep process in the temperature range 220–460°C. The first endothermic reaction occurs at 240°C along with an observed mass loss of 6.45% (Table 1) which is due to the evolution of $8H_2O$. This leads to the conclusion that, after the liberation of coordinated water molecules at 180°C, dehydration of citrate groups to form metal aconitates takes place at about 240°C [18].

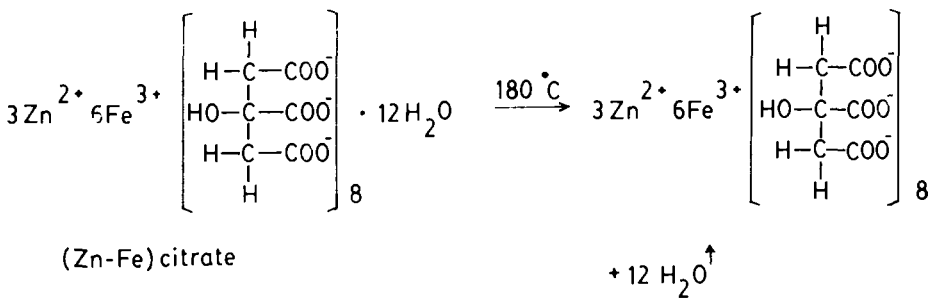

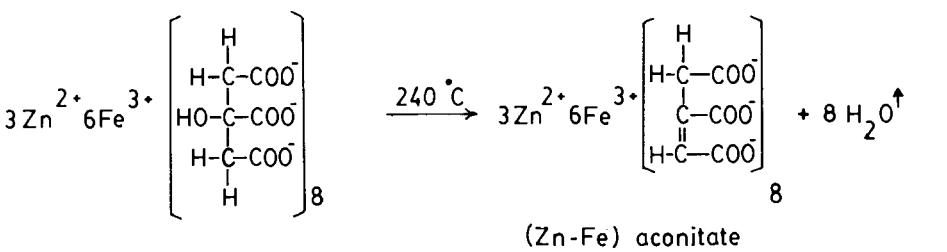

The second step of citrate decomposition occurs in the temperature range 260–460°C with total mass loss of 50.02%, and one endotherm at 285°C and one exotherm at 420°C. At this stage, decomposition is a complex set of reactions which involve dissociation of aconitates, including decarboxylation with evolution of CO and large amounts of H_2O and CO_2, and the oxidation of carbon in air to CO_2, which was produced during the disproportionation of CO. Oxidation of the methylene proton results in the evolution of water vapour. The gas analysis showed that the reaction involves simultaneous evolution of CO_2 and CO. In the temperature

range 260–320°C, the DTA shows a strongly endothermic process indicating the evolution of CO_2 and H_2O. The loss in mass corresponds to evolution of 30 moles of water accompanied by CO_2 and CO gases from two moles of aconitate (from the gas analysis). The residue shows the IR spectrum corresponding to formation of hydrozincite [$Zn_5(CO_3)_2 \cdot 6(OH)$]. XRD studies confirm the presence of hydrozincite, $ZnCO_3$, and also FeO·OH phases where the latter phase exists as $2\alpha\text{-FeO}\cdot\text{OH} \rightleftharpoons \alpha\text{-}Fe_2O_3 + H_2O$.

The shoulder-like exotherm at 420°C in the DTA studies indicates the possibility of rearrangement in the α-Fe_2O_3 structure to give γ-Fe_2O_3. The decomposition of hydrozincite is an endothermic process and leads to the formation of ZnO with the evolution of CO_2 and H_2O [19]. The total mass loss of 4.55% in the temperature range 320–460°C corresponds to the evolution of CO_2 and H_2O from the hydrozincite and FeO·OH decomposition. When the residue obtained in the range 320–460°C (black in colour) is dissolved in concentrated HCl, undissolved black particles are seen confirming the presence of carbon in samples heated to high temperature. The residue obtained in the temperature range 320–460°C consists essentially of ZnO and Fe_2O_3 with traces of CO_2 trapped in the lattice.

In DTA studies (Fig. 1), one endothermic peak and one exothermic peak are noted in the ranges 460–560°C (peak temperature 520°C) and 560–680°C (peak temperature 620°C) respectively. In the temperature range 460–560°C, the formation of $ZnFe_2O_4$ phase is initiated by the solid state diffusion process, $ZnO + Fe_2O_3 \rightleftharpoons ZnFe_2O_4$, which is detected from XRD studies (Fig. 2). And this $ZnFe_2O_4$ phase grows at the expense of ZnO and Fe_2O_3 phases, which is shown by the decrease in the intensity of diffraction lines related to ZnO and Fe_2O_3 phases (Fig. 2). The mass loss at this stage corresponds to 0.97% which can be attributed to the loss of CO_2. The exotherm at 620°C indicates that there is a rearrangement in the $ZnFe_2O_4$ lattice and also oxidation of trapped traces of carbon.

3.5. IR spectral studies of decomposition of the citrate precursor

The assignments of IR bands of the citrate precursor and the decomposition intermediates are shown in Tables 2 and 3. The citrate precursor has all the common bands of citric acid and iron(III) citrate which are listed in Table 2. The shift in IR bands of the precursor compound, as compared to citric acid and iron citrate, indicates the formation of a new complex molecule. The band in the region 3600–3000 cm^{-1} could be due to the presence of water, as the intensity of this absorption line decreases and disappears as the heat treatment temperature increases. Similarly, the bending mode of water at 1610 cm^{-1} decreases in intensity as the heat treatment temperature increases. The absorptions of the citrate precursor at 1720, 1561, 1440 and 1255 cm^{-1} are given in Table 3. The citrate precursor dehydrated at 180°C shows peak absorptions at 3239, 3412 and 1611 cm^{-1}, indicating the loss of coordinated water molecules. The band at 1255 cm^{-1} appears to be due to the formation of a metal hydroxo complex (δ(MOH) bending mode). This band becomes weaker and finally disappears at 420°C. At 240°C, the decomposition of the citrates begin (Fig. 1) as indicated by the weakening of all the IR bands except those at

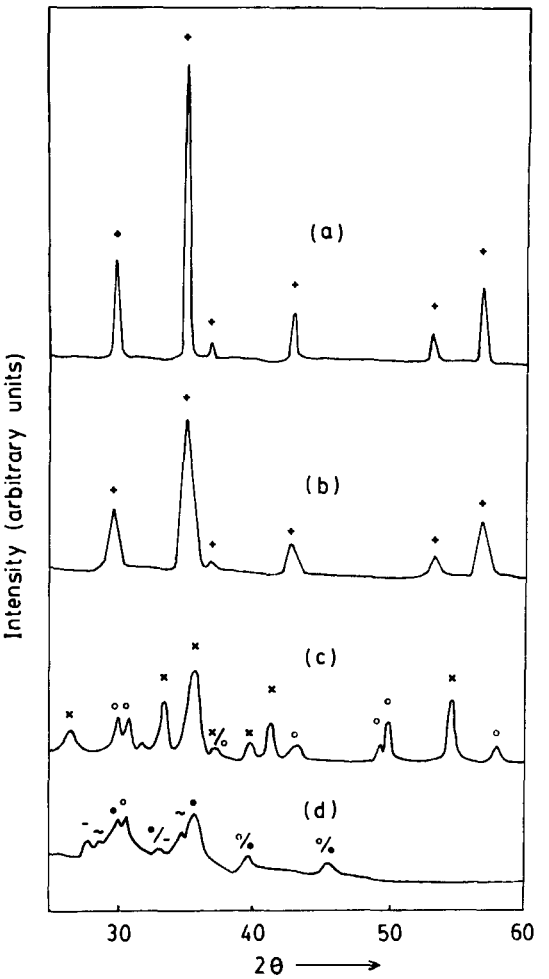

Fig. 2. XRD patterns of $ZnFe_2O_4$ and intermediates obtained at various temperatures: (a) 620°C; (b) 520°C; (c) 420°C; and (d) 285°C. Key: +, $ZnFe_2O_4$; ×, ZnO; ○, Fe_2O_3; –, $ZnCO_3$; ~, $Zn_5(CO_3)_2 \cdot 6(OH)$; and ●, FeO·OH.

1611 and 1440 cm^{-1}. At this temperature, the citrate precursor retains its citrate backbone, except that the loss of a water molecule results in formation of metal aconitates [18]. In the temperature range 260–320°C, methylene protons are oxidized as confirmed by the disappearance of the bands in the range 2956–2847 cm^{-1} and the ν(COO) carboxylate bands at 1440 and 1561 cm^{-1} become very weak, indicating the beginning of the decomposition of the metal aconitates. The band observed at 1611 cm^{-1} for δ(HOH) indicates the formation of hydrozincite and FeO·OH. In the range 260–320°C, the citrate group is completely oxidized, which explains the absence of ν(CH), ν_{asy}(C=O), $\nu(COO^-)$ (or $\nu_{sym}(CO_3)$) in the IR spectrum of the intermediate

Table 2
IR spectral frequency assignments of various compounds (in cm^{-1})

Citric acid	Iron(III) citrate	Precursor	Assignments
3497(vs)	3403(s)	3412(s)	ν(OH) hydroxyl
3291(vs)	3239(br)	3239(br)	ν(OH) water
2913–2847(br)	2956(s)	2956–2847(br)	ν(CH)
1748(vs), 1705(vs)	1729(s)	1720(s)	ν_{asym}(C=O)
	1610(s)	1611(s)	δ(HOH)
	1559(s)	1561(s)	ν(COO) carboxylate
1426(s), 1309(s)	1437(s), 1393(sh)	1440(vs), 1390(s)	ν_{sym}(COO)
1239–1140(s)	1260–1195(br)	1255(m)	δ(MOH)
1086–1065(sh)	1116(m)	1081(m)	Citrate
942(s)	978–956(vw)	987(sh)	
775(vs)	804(m)	851(s), 804(vw)	
640(m)	673(sh)	652(sh)	
597(m)	565(sh)	609(s)	

Key: vs, very strong; s, strong; br, broad; m, medium; sh, shoulder, w, weak; vw, very weak.

obtained in this temperature range. At this stage the absorptions at 1508, 1104 and 871 cm^{-1} ($\nu(CO_3)$) also indicate the formation of hydrozincite and zinc carbonate. These absorptions vanish completely at 420°C, indicating the decomposition of carbonates to form oxides.

The IR spectra of the intermediate compounds obtained at 420 and 520°C have a weak band at 2360 cm^{-1} which is due to the asymmetric stretching mode of free CO_2, suggesting its presence in a trapped state within the matrix. This band disappears when the compounds are heated above 620°C.

3.6. *X-ray diffraction*

X-ray powder diffractograms of the residues obtained at different stages show characteristic diffraction patterns (Fig. 2). The XRD of the residue obtained at 285°C (Fig. 2d) shows characteristic lines for hydrozincite, zinc carbonate and FeO·OH. The residue obtained at 420°C (Fig. 2c) shows characteristic lines for Fe_2O_3 and zinc oxide. As the temperature is increased, the solid state reaction between Fe_2O_3 and ZnO (being highly reactive particles) leads to the formation of $ZnFe_2O_4$ (major phases) at 520°C (Fig. 2b). The solid state reaction is completed around 560°C giving 100% $ZnFe_2O_4$, which is indicated in the XRD pattern. Theoretically, the loss of mass for complete conversion of the citrate pecursor to $ZnFe_2O_4$ is 67.98%, which is comparable to the mass loss observed from TG data (67.90%). Above 620°C (Fig. 2a), the XRD pattern of the products exhibits strong reflections indicating the presence of a well-crystallized single phase of $ZnFe_2O_4$. Thermal decomposition is accompanied by growth in particle size which is indicated by the increase in the sharpness of the lines in the XRD patterns of $ZnFe_2O_4$.

Table 3
IR spectral frequency assignments for $Zn_3Fe_6(C_6H_5O_7)_8 \cdot 12H_2O$ and decomposition products (in cm^{-1})

Assignment	80°C	180°C	240°C	280°C	420°C	520°C	620°C
ν(OH) hydroxyl	3412 (s)	3412 (br)	3412 (br)	3412 (br)	3412 (br)	–	–
ν(OH) water	3239 (br)	3239 (br)	3239 (br)	3239 (br)	3239 (br)	3239 (w)	3239 (vw)
ν(CH)	2956–2847 (br)	2956–2847 (w)	2956–2847 (w)	–	–	–	–
$\nu(CO_2)$	–	–	–	–	2360 (w)	2360 (w)	2360 (w)
ν_{asym}(C=O)	1720 (s)	1720 (sh)	1720 (w)	–	–	–	–
δ(HOH) water	1611 (s)	1611 (m)	1611 (m)	1611 (m)	1611 (w)	1611 (vw)	1611 (vw)
ν_{asym}(COO) carboxylate	1561 (s)	1561 (s)	1561 (m)	–	–	–	–
$\nu(CO_3)$ carbonate	–	–	–	1508 (w)	–	–	–
ν_{sym}(COO)	1440 (s)	1440 (s0	1440 (s)	–	–	–	–
$\nu_{sym}(CO_3)$ carbonate	–	–	–	1390 (m)	–	–	–
δ(MOH)	1255 (m)	1255 (w)	1255 (vw)	1255 (vw)	–	–	–
Citrate	1117 (s)	1117 (s)	1117 (s)	–	–	–	–
$\nu(CO_3)$	–	–	–	1104 (m)	–	–	–
Citrate	1080 (m)	1080 (m)	1080 (sh)	–	–	–	–
Citrate	987 (sh)	987 (sh)	987 (sh)	–	–	–	–
$\nu(CO_3)$	–	–	–	871 (m)	–	–	–
Citrate	847 (m)	847 (m)	847 (w)	847 (m)	–	–	–
ν(Fe–O)	655 (sh)	655 (sh)	655 (sh)	655 (sh)	655 (sh)	655 (sh)	655 (sh)
	607 (m)	607 (s)	607 (s)	607 (s)	607 (m)	607 (m)	607 (m)

Key: s, strong; br, broad; m, medum; w, weak; vw, very weak; sh, shoulder.

4. Discussion

The following scheme represents the probable course of the decomposition reaction of the citrate precursor, $Zn_3Fe_6(cit)_8 \cdot (12 + n)H_2O$, in the temperature range 25–700°C in air atmosphere.

1. $Zn_3Fe_6(C_6H_5O_7)_8 \cdot (12+n)H_2O \xrightarrow{25^\circ - 120^\circ C} Zn_3Fe_6(C_6H_5O_7)_8 \cdot 12(H_2O) + nH_2O\uparrow$

   (Zn-Fe) citrate precursor

2. $Zn_3Fe_6(C_6H_5O_7)_8 \cdot 12(H_2O) \xrightarrow{120^\circ - 220^\circ C} Zn_3Fe_6(C_6H_5O_7)_8 + 12H_2O\uparrow$

3. $Zn_3Fe_6(C_6H_5O_7)_8 \xrightarrow{220^\circ - 260^\circ C} Zn_3Fe_6(C_6H_3O_6)_8 + 8H_2O\uparrow$

   metal aconitate

4. $2[Zn_3Fe_6(C_6H_3O_6)_8] \xrightarrow{260^\circ - 320^\circ C} Zn_5(CO_3)_2 \cdot 6(OH) + ZnCO_3 + 12FeO \cdot OH$

   hydrozincite

   $+ 30H_2O\uparrow + 81CO_2\uparrow + 12CO\uparrow$

5. $Zn_5(CO_3)_2 \cdot 6(OH) + ZnCO_3 \xrightarrow{320^\circ - 460^\circ C} (ZnO)_6 \cdot CO_2 + (Fe_2O_3)_6 \cdot CO_2 + 2CO_2\uparrow$

   $+ 12FeO \cdot OH \qquad + 9H_2O\uparrow$

6. $(ZnO)_6 \cdot CO_2 + (Fe_2O_3)_6 \cdot CO_2 \xrightarrow{460^\circ - 560^\circ C} (ZnFe_2O_4)_6 \cdot CO_2 + CO_2\uparrow$

7. $(ZnFe_2O_4)_6 \cdot CO_2 \xrightarrow{560^\circ - 680^\circ C} 6ZnFe_2O_4 + CO_2\uparrow$

The first step represents the removal of extra adsorbed water molecules, and the second represents the loss of coordinated water molecules. The third step corresponds to evolution of H_2O from the citrate lattice, leading to the formation of metal aconitates. The fourth step corresponds to the complete conversion of metal aconitates to hydrozincite, zinc carbonate and FeO·OH.

The fifth step corresponds to the formation of ZnO and Fe_2O_3 (with evolution of CO_2 and H_2O). The sixth step represents the formation of $ZnFe_2O_4$. In the DTA curve, the exothermic peak corresponding to the seventh step is attributed to (i) the rearrangement in the $ZnFe_2O_4$ lattice, and (ii) the oxidation of carbon which was produced during disproportionation of CO gas. It was further observed that the carbon residue disappeared completely on keeping the samples above 620°C for more than seven days. It is quite probable that the composition obtained has phases which are extremely divided mixtures of Fe_2O_3 and ZnO and which on undergoing solid state reaction lead to the formation of single spinel $ZnFe_2O_4$ phase at low temperature, because of the fact that fine particles have greater reactivity. The XRD pattern (of the product obtained at 520°C) showed broad characteristic lines for the crystalline $ZnFe_2O_4$ phase (Fig. 2b).

The crystallite size was determined from the X-ray pattern using the Debye-Scherrer equation

$$D_{hkl} = \frac{K\lambda}{\beta \cos\theta}$$

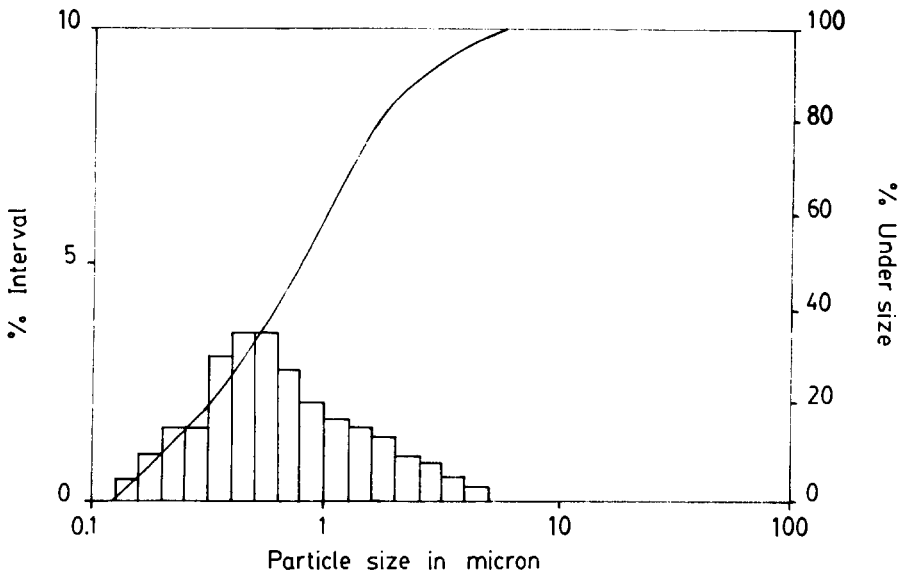

Fig. 3. Particle size distribution curve for $ZnFe_2O_4$ synthesized by precursor technique.

where D_{hkl} is the particle diameter in nanometers, K the shape factor (≈ 0.9) and β the corrected line width in radians ($\beta = \beta'_{obs} - \beta''_{ref}$). The crystallite size calculated from X-ray line width was seen to be in the range 10–11 nm. Quartz powder was used as reference material.

The average agglomerate size of zinc ferrite obtained by the citrate precursor technique measured using a Horiba LA-500 particle size analyser was seen to be around 0.65 μm..

5. Conclusions

Fine-particle $ZnFe_2O_4$ was synthesized by a citrate precursor technique. The mechanism of the thermal decomposition of the citrate precursor in air was established. The high decomposition rate, low decomposition temperature and the dissipation of heat due to evolution of large amounts of gaseous products resulted in formation of $ZnFe_2O_4$ with crystallite sizes ranging from 10 to 11 nm. With the increase in heat treatment temperature, the crystallinity of the sample was observed to increase (sharper X-ray lines). Study by the particle size analyser showed the presence of agglomerates with average size of 0.65 μm.

Acknowledgements

VSD thanks the Council of Scientific and Industrial Research New Delhi for financial support. UB gratefully acknowledges the award of fellowship by the Department of Atomic Energy, Government of India.

References

[1] P.I. Slick, Ferrites for Non-Microwave Applications, p. 189.
S.W. Charles and J. Popplewell, in E.P. Wohlfarth North (Ed.), Ferromagnetic Materials, Holland Publishing Company, New York, Vol. 2, 1980, p. 509.
[2] C.A. Leech III and L.E. Campbell, in R.F. Gould (Ed.), Spinel Solid Solution Catalysts for Automotive Applications, American Chemical Society, Washington D.C., 1975, p. 161.
[3] G.R. Dube and V.S. Darshane, J. Chem. Soc. Faraday Trans., 88 (1992). 1299.
[4] G.R. Dube and V.S. Darshane, Bull. Chem. Soc. J., 64 (1991) 2449.
[5] D.W. Johnson, Jr., Am. Ceram. Soc. Bull., 60 (1981) 221.
[6] P.M. Khopkar, J.A. Kulkarni and V.S. Darshane, Thermochim. Acta, 93 (1985) 481.
[7] A. Clearfield, A.M. Gadalla, W.H. Marlow and T.W. Livingston, J. Am. Ceram. Soc., 72 (1989) 1782.
[8] B.J. Ingrebrethsen and E. Matejević, J. Colloid Interface Sci., 100 (1984) 1.
[9] B.A. Mulla and V.S. Darshane, Ind. J. Chem., 22A (1983) 143.
[10] W.J. Schuele and V.D. Dectscreek, Fine particle Ferrites, in W.E. Kuhn, H. Lamprey and C. Sheer (Eds.), Ultrafine Particles, Wiley, New York, 1963, p. 218.
[11] P. Ravindranathan and K.C. Patil, Am. Ceram. Soc. Bull., 66(4) (1987) 688.
[12] V.K. Sankaranarayan and N.S. Gajbhiye, Thermochim. Acta, 153 (1989) 337.
[13] V.K. Sankaranarayan and N.S. Gajbhiye, J. Am. Ceram. Soc., 73 (1990) 1301.
[14] A.I. Vogel, A Textbook of Quantitative Inorganic Analysis', 3rd edn., Longmans, London, 1962.
[15] D.C. Garratt, The Quantitative Analysis of Drugs, 3rd edn., Chapman and Hall Ltd., London, 1964.
[16] H.P. Klug and L.E. Alexander, X-Ray Diffraction Procedures, Wiley, New York, 1954.
[17] National Bureau of Standards (USA), Monograph 25, Section 9, 1971.
[18] D. Hennings and W. Mayr, J. Solid State Chem., 26 (1978) 329.
[19] C.W. Beck, Thesis, Harvard University, Cambridge, Massachusett, USA, 1946.